sustainability

Article

Organic Matter of the Wufeng–Longmaxi Formation Shales Using Scanning Electron Microscopy

Jing Wang [1,2], Fawang Ye [1], Gary G. Lash [3] and Zhaodong Xi [2,*]

[1] National Key Laboratory of Remote Sensing Information and Image Analysis Technology, Beijing Research Institute of Uranium Geology, Beijing 100029, China
[2] School of Energy Resource, China University of Geosciences (Beijing), Beijing 100083, China
[3] Department of Geology and Environmental Sciences, State University of New York—Fredonia, Fredonia, NY 14063, USA
* Correspondence: xizhaod@cugb.edu.cn

Abstract: Fine-grained organic matter (OM) particles are commonly widely dispersed in shale deposits. However, carrying out investigations of pores hosted by OM particles and the nature of grain interactions in OM particles and associated detrital grains using optical microscopy is difficult at best. Scanning electron microscopy (SEM) is much better suited for characterizing the microstructure of dispersed OM particles and has found wide application in the study of unconventional oil and gas systems. Scanning electron microscopy was used to define the types of OM contained in marine shale deposits of the Wufeng and Longmaxi Formations spanning the Ordovician–Silurian transition in South China. Of particular interest was the development of OM-hosted pores and the identification of the factors that controlled their formation. The dominant OM type contained in the studied deposits is pyrobitumen, with subordinate graptolitic OM and sparse OM of unknown origin. Pyrobitumen is present in four forms, including pore fillings among authigenic quartz grains, within framboidal pyrite, and between authigenic clay grains and massive material. Diagenetic alteration has given rise to OM pores of differing morphology, size, and time of formation. Common small, equisized circular or oval OM pores are most developed and appear to have formed in association with the generation of hydrocarbons. Shale deposits containing abundant pyrobitumen filling interparticle pores among authigenic quartz crystals display robust reservoir and fracturing capacity. A sedimentary environment appears to have been the main factor affecting the type of OM and the nature of its association with detrital and authigenic minerals. Results of this study demonstrate that a sedimentary environment is a primary requisite for the formation of highly prospective/high-yielding hydrocarbon shale reservoir deposits.

Keywords: shale gas; organic matter; SEM; pyrobitumen; organic pore

check for updates

Citation: Wang, J.; Ye, F.; Lash, G.G.; Xi, Z. Organic Matter of the Wufeng–Longmaxi Formation Shales Using Scanning Electron Microscopy. *Sustainability* **2023**, *15*, 13438. https://doi.org/10.3390/su151813438

Academic Editors: Jingshou Liu, Lei Gong and Wei Ju

Received: 21 June 2023
Revised: 21 August 2023
Accepted: 23 August 2023
Published: 7 September 2023

1. Introduction

With the continuous growth of the global energy demand and the increasing call for environmental protection and sustainable development, shale gas, as a highly regarded alternative energy source, has gradually become a star in the energy industry. The abundance of organic matter (OM), the thermal maturity of OM, and the type of OM are important parameters for evaluating the hydrocarbon generation potential and reservoir capacity of shale [1–4]. However, the influence of the OM type on shale gas reservoir evolution and capacity characteristics requires further detailed analysis. OM types are commonly described in relation to the types of kerogen at present. Kerogen types can be described in terms of the atomic ratios of C, H, and O and the results of rock pyrolysis [5–7]. Different kerogen types reflect the dominant sources of OM [8]. For example, Type III kerogen is derived from higher plants, mainly vitrinite and inertinite, whereas Type I kerogen is normally sourced from lower organisms, mainly the sapropelic group. Thus, different kerogen types contain a variety of macerals.

OM particles in shale are widely dispersed and fine grained. Although macerals in shale can be identified using optical microscopy, the details of OM pore development and the nature of OM particles and detrital and authigenic minerals (e.g., quartz), reservoir rock aspects critical of shale gas reservoir consideration, are difficult to observe [9–13]. Scanning electron microscopy (SEM), by virtue of great magnification, clear image quality, and three-dimensional imaging capacity, has greater research potential than optical microscopy. SEM has been widely used in the study of OM pores, mineral types, and diagenesis in shale deposits.

Distinguishing OM types in shale using SEM has important implications for understanding the evolution of pores hosted by OM. This study attempts to address problems associated with the identification of the OM type using SEM observations by studying marine shale deposits of the Wufeng and Longmaxi Formations characterized by abnormally high proportions of single-maceral material. The implications of our results for shale gas exploration and development are also addressed.

2. Definition and Classification of OM Types Based on SEM

"Organic matter" is a general term that refers to any liquid or solid substance rich in organic carbon. In fact, commonly used terms, such as "vitrinite," "kerogen," "asphalt," and "solid bitumen," are all expressions for different types of OM [14]. Numerous SEM-based OM classification schemes have been proposed (Table 1). However, at present, there is still no universally accepted standard.

Table 1. Nomenclature of OM types using SEM and their corresponding description/interpretation.

OM Types	Description/Interpretation	Related References [11,13,15–18]
Scattered OM	OM locally rich and showing block (a few or dozens of microns) distribution, dispersed among the matrix	Zhang et al., 2015; Xi et al., 2019 [13,15]
Striped OM	OM and minerals alternately deposited, with OM being strip shaped	
Interstitial OM	OM filling in pores between minerals, having no definite shape	
Depositional OM	The primary OM and its alteration products, which have not migrated, mainly include kerogen and its evolved solid bitumen or pyrobitumen.	Loucks and Reed, 2014; Zhao et al., 2017 [16,17]
Migrated OM	Bitumen or petroleum existing in pores and migrated from other places can evolve into solid bitumen or pyrobitumen with an increase in thermal maturity.	
Detrital OM	Originating as particulate detritus present at the time of deposition	Milliken et al., 2014 [11]
Secondary OM	OM generated as a diagenetic product during burial	
Unknown OM	OM of uncertain origin	
Structured OM	OM with a special structure or an obvious boundary with surrounding minerals	Camp, 2019 [18]
Amorphous OM	Corresponding to structural OM, it lacks any definite form and often surrounds minerals.	
Void-filling OM	OM filled in pores as cement	

The general standards used in the classification of OM types using an optical microscope, such as the Chinese Oil and Gas Industry Standard "Methods of transmission light-fluorescence kerogen maceral identification and classification (SY/T5125)" and "Maceral identification and statistical method of whole rock optical slice (SY/T6414)" and National Standards "Maceral classification of bituminous coal (GB/T15588)" and the TSOP/ICCP classification of dispersed OM in sedimentary rocks [19].

This study adopts the OM type classification scheme presented in Figure 1. Specifically, OM is first classified as primary OM or secondary OM. Optical characteristics are used to classify primary OM into sapropelic, liptinite, vitrinite, and inertinite groups or zooclasts. Secondary OM is classified as solid bitumen or pyrobitumen. Solid bitumen has been considered secondary OM generated in the oil window. It has also been referred to as pre-oil solid bitumen by some authors [20,21], whereas pyrobitumen has been regarded as secondary OM produced during the generation of gas. Pyrobitumen has been referred to as post-oil solid bitumen by some scholars [20,21]. The surge in scientific interest in and the study of shale gas have forced researchers to rethink the nomenclature and classification of OM [22]. Thus, it is important to achieve some degree of uniformity in OM nomenclature in order to reduce confusion when describing the OM type [22–24]. Because the nomenclature and classification of OM types based on optical microscopy have been widely adopted, the classification scheme and nomenclature of OM types based on SEM should also be the same (Figure 1).

	Primary organic matter (from depositional setting)	Secondary organic matter (from transformation of primary organic matter)
Organic Petrology	Macerals (sapropelinite, liptinite, vitrinite, intertinite)	Solid bitumen
	Organic zooclasts (e.g. graptolite)	Pyrobitumen

Figure 1. Basic nomenclature of OM used in this study (modified after [14]).

3. Samples and Methods

Organic-rich strata of the Wufeng and Longmaxi Formations were deposited in late Ordovician and Early Silurian times on the upper Yangtze Platform of south China [3,25]. Core samples obtained from the southeastern edge of the Sichuan Basin in northwestern Hunan were selected as the focus for the investigation (Figure 2a). These deposits were selected for study for the following reasons: (i) They are rich in OM and have been commercially developed, and relevant geological research has been carried out at a sufficient level of detail [26–30], and (ii) according to the color, transparency, size, shape, protrusion, and fluorescence of OM, the OM type can be well distinguished under an optical microscope. However, it is difficult to study the OM type using SEM, as the low atomic weight of carbon makes all the OM appear dark black. The OM of the Wufeng and Longmaxi Formations is mainly sourced from lower organisms (Type I kerogen), and vitrinite reflectance equivalent values of greater than 2.0% suggest over-mature thermal maturity. Thus, most OM types of these deposits are therefore pyrobitumen [31–34]. Therefore, it can be considered that the OM observed using SEM is basically pyrobitumen. Based on this, the petrological characteristics of pyrobitumen can be analyzed, which provides a good guiding significance for distinguishing the OM types and the development of OM pores using SEM.

Shale samples were selected from core material recovered from well X3 in northwestern Hunan (Figure 2b). Shale samples were analyzed using SEM, as described in papers published by our team [35,36].

Total organic carbon (TOC) contents of the Wufeng Formation and the lower Longmaxi Formation in the study area are similar (Table 2) and average 1.47% and 1.36%, respectively. The TOC content of the upper Longmaxi Formation is relatively low and averages 0.32%. Analyzed samples of the Wufeng Formation and the lower Longmaxi Formation are dominated by quartz (Table 2; average = 50.1%), followed in abundance by clay minerals, feldspar, pyrite, and carbonate minerals (Table 2). Clay minerals are dominant in samples of the upper Longmaxi Formation (average = 50.0%), with lesser abundances of quartz and feldspar. Pyrite and carbonate minerals are present but at low concentrations.

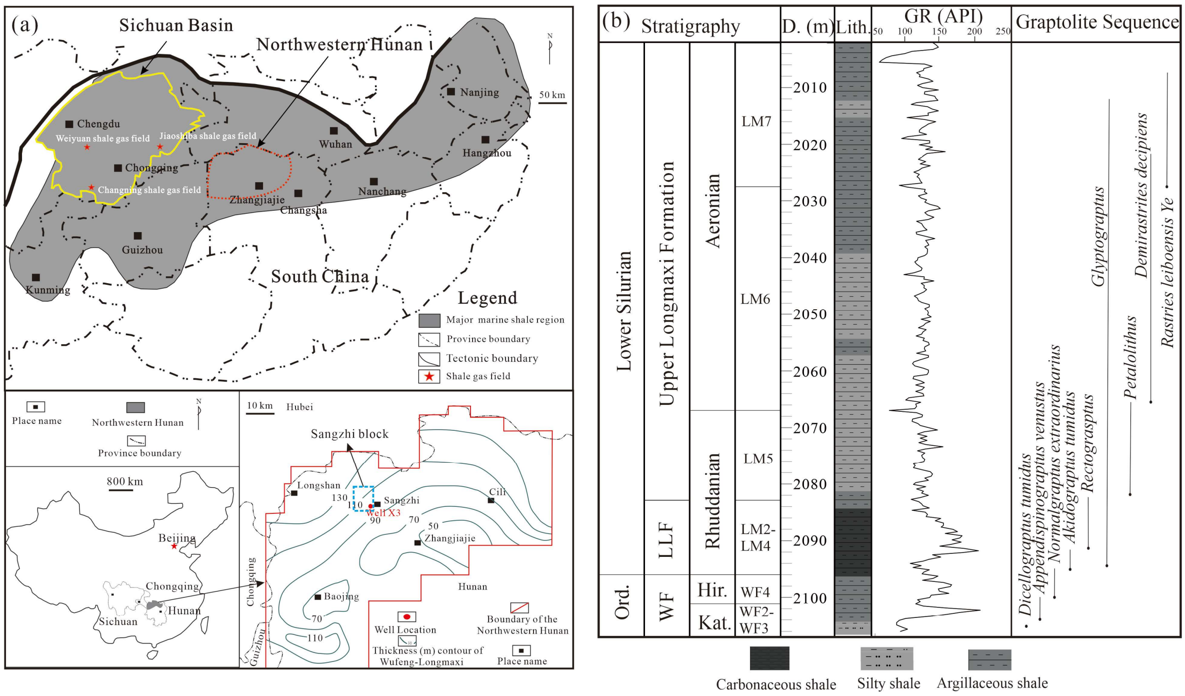

Figure 2. (**a**) The location of sampling well X3 in northwestern Hunan. (**b**) A comprehensive stratigraphic column for well X3 (modified after [35]).

Table 2. TOC content and mineral compositions of analyzed Wufeng–Longmaxi samples of well X3.

Formation	TOC (%)	TOC Average (%)	Quartz (%)	Clay (%)	Calcite (%)	Dolomite (%)	K-Feldspar (%)	Albite (%)	Pyrite (%)	Clay Types (%)	
										Illite	I/S
Upper Longmaxi	0.15	0.32	42.6	47.6	/	/	0.9	8.9	/	97	3
	0.18		39.2	50.4	/	/	1	9.4	/	94	6
	0.16		38	53.2	/	/	/	8.8	/	90	10
	0.24		38.4	48.4	/	/	/	9.4	1.2	93	7
	0.65		36.1	52.1	/	/	/	9.2	0.7	90	10
	0.16		38.7	49.7	/	/	/	9.6	0.4	80	20
	0.22		35.3	53	/	/	0.9	8.9	0.4	89	11
	0.30		37.6	50.2	/	/	/	9.9	0.4	83	17
	0.14		37	51.2	/	/	1.1	9.2	0.2	82	18
	0.17		39.4	49.2	/	/	/	9.8	0.2	96	4
	1.17		37.3	44.5	/	/	3	9.3	1.9	96	4
Lower Longmaxi	1.42	1.36	39.2	45.8	/	/	/	10.7	3.9	96	4
	1.75		32	35.7	/	12.1	3.7	8.2	5.4	95	5
	1.68		43.1	30.6	2.3	9.9	4	10.1	/	85	15
	1.44		44.1	26	2.3	10.2	2.8	9.7	3.1	91	9
	1.04		38.6	36.4	2.5	11.4	2.2	8.9	0	92	8
	1.19		42.2	28.5	2.2	11.2	1.9	10.9	1.6	90	10
	1.02		41.3	27.4	2.1	10.8	5.3	9.9	1.9	82	18
	1.52		35.2	33.4	/	10.9	2.4	10.8	5.5	94	6
	1.30		37.1	25	9.9	7.2	4.8	13	1.6	97	3
	1.29		42.1	31.3	/	7.1	3.9	12.3	1.8	88	12
Wufeng	0.96	1.47	45.6	23.4	7.6	5.3	4.4	11.6	0.9	87	13
	1.28		45.6	24.3	/	9.1	2.7	12.6	3.9	95	5
	1.25		42.6	22.7	7.5	8.3	3.5	12.9	1.2	89	11
	0.73		44.2	34.2	/	8.9	3.8	7.2	0.8	93	7
	1.36		56.7	22.6	/	13.4	1.3	4.8	0.4	95	5
	1.57		58.9	30.7	/	/	1.8	6.6	0.7	95	5
	1.29		64.7	26.3	/	/	1.7	5.8	0.5	85	15
	2.19		86.4	8.7	2.8	/	0.8	1.3	/	88	12
	1.59		79.7	15.2	1.2	/	0.9	3	/	96	4
	2.28		49.2	34.7	/	6	2	5.8	0.9	96	4
	1.38		70.4	18.1	1.9	4.2	1	3.1	0.6	97	3
	1.86		63.1	24.5	2.7	3.1	1.4	5.2	/	96	4

Note: I/S = illite/smectite mixed layer; / = not detected.

4. Results and Discussion

4.1. OM Assemblages

Optical microscopy suggested that the OM of the studied samples is dominated by variably shaped pyrobitumen (Figure 3a,b). Graptolites (zooclasts) were observed occasionally in some samples (Figure 3c,d).

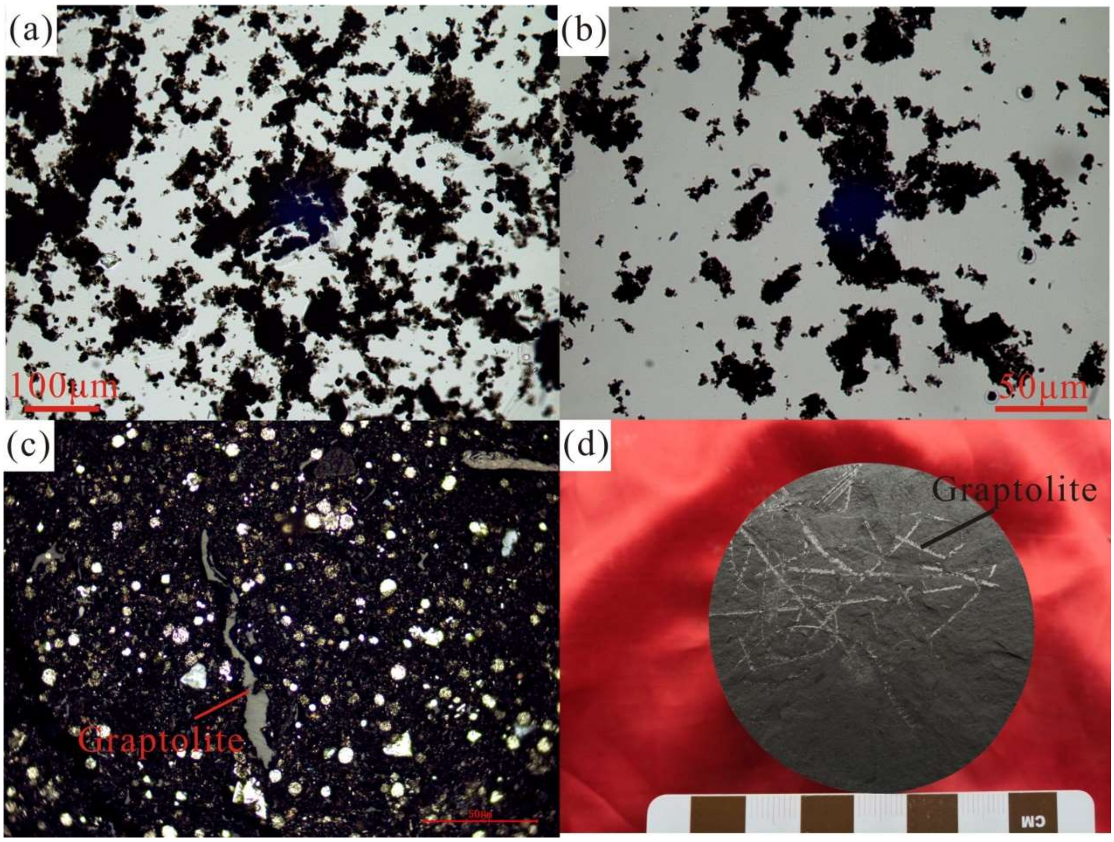

Figure 3. OM of the Wufeng–Longmaxi shale samples: (**a**,**b**) kerogen concentrates (dark material) under transmitted light. The observed OM is mainly pyrobitumen that lacks an obvious shape and structure. (**c**) One graptolite particle under reflected light using an oil immersion; (**d**) core sample containing abundant graptolites.

Results of some SEM-based studies suggest that although pyrobitumen is the dominant OM type in the Wufeng–Longmaxi Formations, subordinate OM similar to inertinite, vitrinite, and degraded algae was also present in the studied samples. The Wufeng and Longmaxi Formations were deposited during the Ordovician–Silurian transition, a time during which higher plants were not well developed, negating the presence of inertinite and vitrinite in the sample set. It is noteworthy that carbon chips (Figure 4a,b) or micrinite ([32]; see their Figure 8) are commonly interpreted as inertinite and vitrinite. The occasional carbon chips observed in the studied samples may reflect the contribution of frequent volcanic eruptions known to have occurred contemporaneous with the deposition of the Wufeng and Longmaxi Formations [37,38]. Carbon chips commonly display smooth, flat surfaces and shell or stepped fractures and have obvious boundaries with surrounding minerals. It is noteworthy, though, that carbon chips lack pores. Micrinite is a relatively heavy product of hydrocarbon generation that is found within secondary OM (e.g., pyrobitumen) ([32]; see their Figure 8). Given that the studied deposits reached the over-mature stage, it is likely that essentially all algae would have been transformed hydrocarbons, though some refractory algal residues appear to have been preserved (Figure 4c,d).

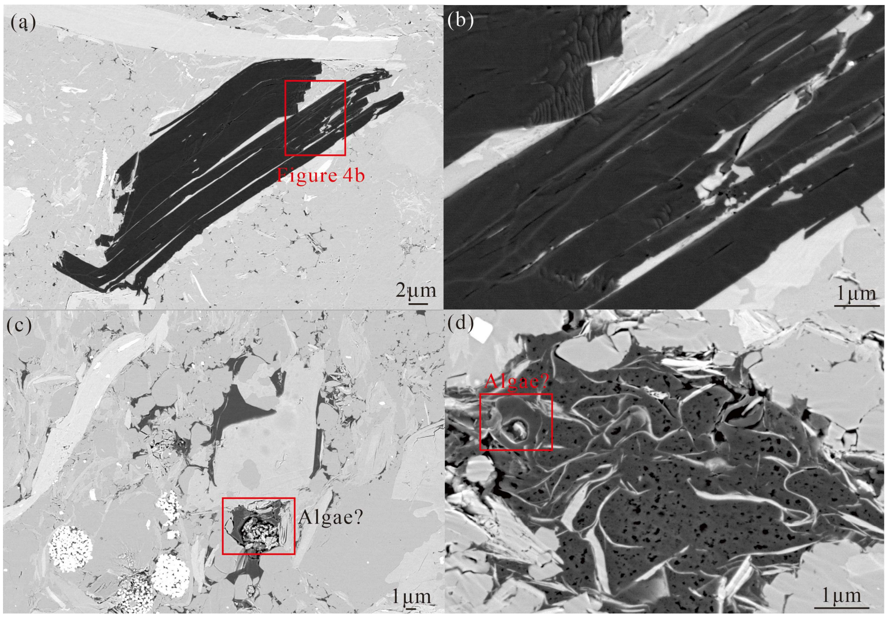

Figure 4. Unknown OM in Wufeng–Longmaxi shale samples viewed using SEM: (**a**,**b**) may show carbon chips perhaps introduced to the sediment by volcanic eruptions; (**c**,**d**) inferred residual algae. The outer wall of algae is difficult to degrade. The cavity is filled with clay minerals.

Carbon chips and degraded algae are generally rare, and their origin needs to be further studied. Therefore, these two types of OM are not discussed further in this study. In summary, the deposits of the Wufeng and Longmaxi samples are dominated by pyrobitumen, with lesser graptolite.

4.1.1. Organic Zooclasts

Organic zooclasts mainly include scolecodonts, graptolites, chitinozoa, and foraminifera in shales. Graptolites flourished during the Ordovician–Silurian transition, thus explaining their great abundance in the studied deposits. Graptolites in the well X3 core display random orientation (Figure 4d). Graptolites viewed using SEM are often striped and can be as long as several to dozens of microns (Figure 5a–c). Graptolite surfaces are generally smooth and flat. The central canal is filled with framboidal pyrite (Figure 5c), with the graptolite sometimes replaced by carbonates (Figure 5a). The theca and sicula of some graptolites have been observed (Figure 5d).

4.1.2. Pyrobitumen

As pointed out in the discussion, with the exception of graptolites, almost all OM in the studied samples is pyrobitumen. Pyrobitumen observed in Wufeng and Longmaxi samples occurs in several forms: (i) Pyrobitumen fills the interparticle pores of authigenic quartz (Figure 6a,b). This type of pyrobitumen is most common in samples enriched in TOC and quartz. Quartz in these samples is mainly authigenic and may comprise more than 50% of the sample [39]. Authigenic quartz crystals are generally 1–5 microns and well formed (Figure 6a,b). The shape of this form of pyrobitumen reflects the shapes of the filled pores suggesting that the pyrobitumen formed after precipitation of the authigenic quartz. (ii) Some pyrobitumen fills the interparticle pores within pyrite framboids (Figure 6c). This type of pyrobitumen is most common to samples enriched in TOC and pyrite. Observed pyrite framboids are generally less than 10 microns, with the 5–8 micron being the most populated. The form of the pyrobitumen is controlled by the shapes of filled pores. Thus, the pyrobitumen likely formed after the framboids formed. (iii) Pyrobitumen is observed to have filled the interparticle pores of authigenic clay minerals (Figure 6d). This type of pyrobitumen has been observed in all samples. Clay minerals are mainly fibrous or plate-like authigenic illite associated with OM. (iv) The final occurrence of pyrobitumen is as massive OM dispersed throughout the clay matrix (Figure 7). Much of this pyrobitumen, which was present in all analyzed samples, is wrapped by detrital clay minerals. Grains of this type of pyrobitumen can reach several microns to more than ten microns in size.

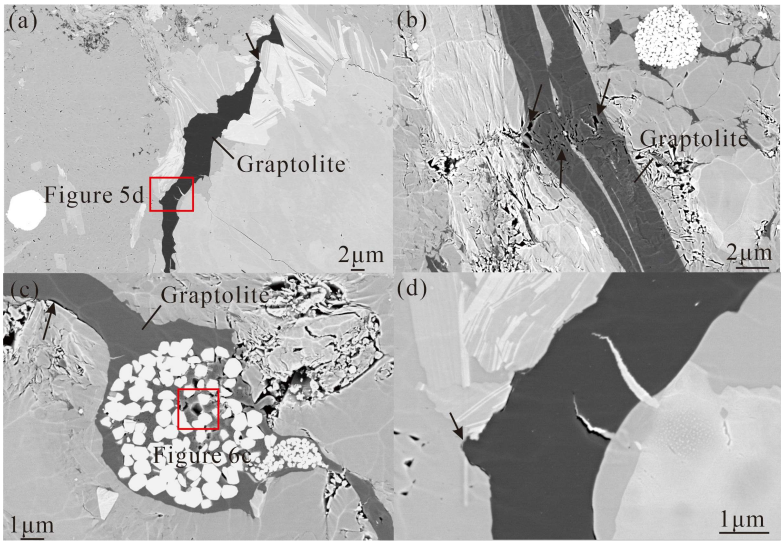

Figure 5. Graptolites hosted by Wufeng–Longmaxi shale samples viewed using SEM: (**a**) graptolites are striped. Black arrows point to the graptolites that have been replaced by carbonates. (**b**) Striped graptolite surrounded by clay minerals. The black arrow points to pores hosted by the graptolite. (**c**) Central canal of a graptolite filled with framboidal pyrite. The black arrow points to pores that formed between the graptolite and minerals. The content in the red box is shown in Figure 6c. (**d**) The black arrow points to the inferred theca and sicula of a graptolite.

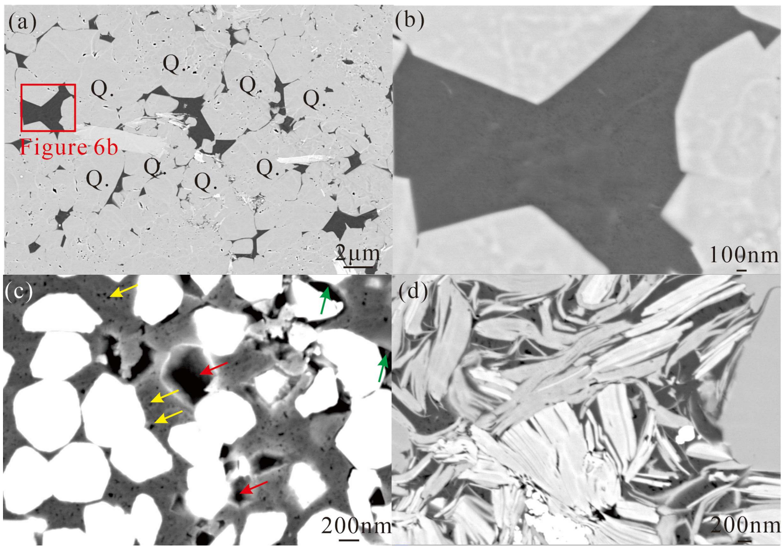

Figure 6. Pyrobitumen of the Wufeng–Longmaxi shale samples viewed using SEM: (**a**) pyrobitumen has filled interparticle pores among authigenic quartz crystals; (**b**) pyrobitumen contains OM pores filling interparticle pores of authigenic quartz; (**c**) pyrobitumen has filled interparticle pores of pyrite framboids. The yellow arrows indicate small, equal-sized, circular or oval-shaped OM pores. The green arrow points to pores between pyrite crystals and OM. The red arrows indicate large pores similar to a single crystal of framboidal pyrite. (**d**) Pyrobitumen has filled interparticle pores in authigenic clay minerals.

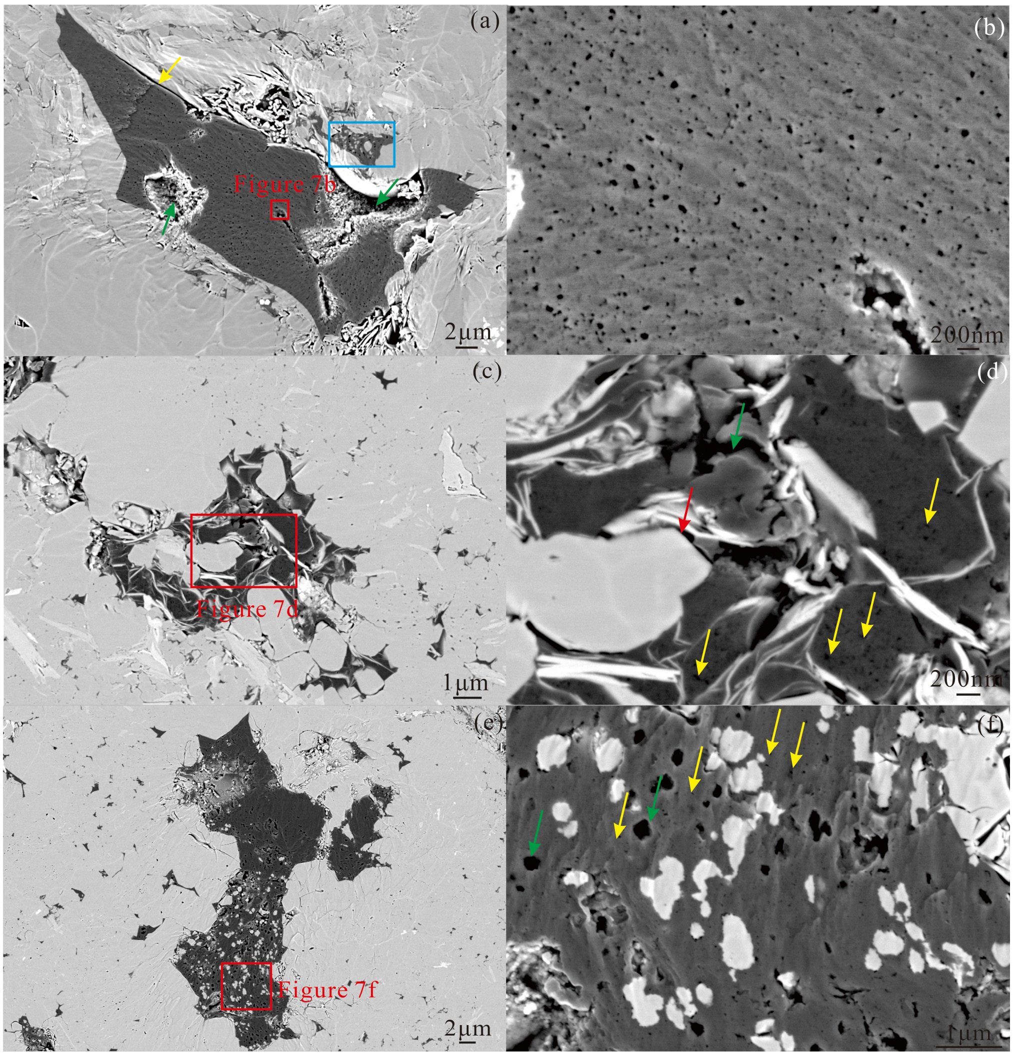

Figure 7. Pyrobitumen in Wufeng–Longmaxi shale samples viewed using SEM: (**a**,**b**) pyrobitumen of a large particle size hosting abundant OM pores. The blue box indicates a small pyrobitumen particle in which most pores are filled with minerals. The green arrow highlights a large irregularly shaped pore that may have formed by dissolution. The yellow arrow indicates pores at contacts of pyrobitumen and surrounding minerals. (**c**,**d**) Pyrobitumen containing abundant OM pores wrapping minerals. The red arrows point to pores at the contacts of OM and wrapped minerals. The green arrows indicate large irregular pores. The yellow arrows point to small, equidimensional, round and oval pores. (**e**,**f**) Large pyrobitumen particles hosting abundant pores, some filled with minerals. The green arrow indicates large OM pores that have been partially filled with minerals. The yellow arrow shows small, equal-sized, round or oval-shaped OM pores.

Pyrobitumen is a viscous fluid product of catagenesis that can migrate through the source rock [14,40]. The first three types of pyrobitumen show evidence of migration. Wood et al. (2018) posited that the massive pyrobitumen containing clay minerals is an internal flow structure related to the entrainment of clay minerals by migrating highly viscous fluid produced by the thermal maturation of OM [41]. However, clay minerals contained in this kind of pyrobitumen of the studied samples do not display preferred orientations, appearing, instead, more like the aggregates of clay grains and OM (Figure 6d). Aggregates of OM and clay minerals are formed by the adsorption of OM onto clay grains during deposition. Increasing thermal maturity would convert the OM into a highly viscous hydrocarbon fluid. It is important to point out that compaction can impart a clay grain texture similar to that expected to form as a result of flow [18]. In summary, then, the fourth type of pyrobitumen documented in the studied Wufeng–Longmaxi samples lacks evidence of migration.

4.2. OM Pores

4.2.1. Pores Hosted by Organic Zooclasts

As graptolites have a specific morphology and structure, they can be readily identified using SEM. We observed two types of pores hosted by graptolites: (i) a series of irregular pores that may have been formed in association with the compaction of graptolites (Figure 5b) and (ii) a second type of pore including those voids at contacts of minerals and graptolites (Figure 5c). These pores may have been formed by shrinkage in association with thermal stress. These two pore types are rarely observed in the studied samples (Figure 5a,d). Graptolites are geochemically similar to Type III kerogen, which contains abundant oxygen-bearing functional and aromatic groups [42]. Therefore, graptolites are characterized by poor hydrocarbon generation ability and contain almost no pores. Some researchers have observed copious pores in fusellar layers of graptolites. The directional arrangement of these pores is controlled by the primary structure of the graptolite. We did not observe such pores in our samples, and such pores are mentioned in other studies, perhaps an indication that these pores are less well developed in general.

4.2.2. Pores Hosted by Pyrobitumen

As described before, four types of pyrobitumen have been recognized in samples of the Wufeng and Longmaxi Formations. Each of these contains OM pores, though the pores differ in terms of morphology, size, and distribution (Figures 6–8). Pyrobitumen filling the interparticle pores of authigenic quartz contains abundant pores that display similar circular or elliptical shapes and sizes, generally at a nanometer level within a range of 5–20 nm (Figures 6a,b and 8a,b).

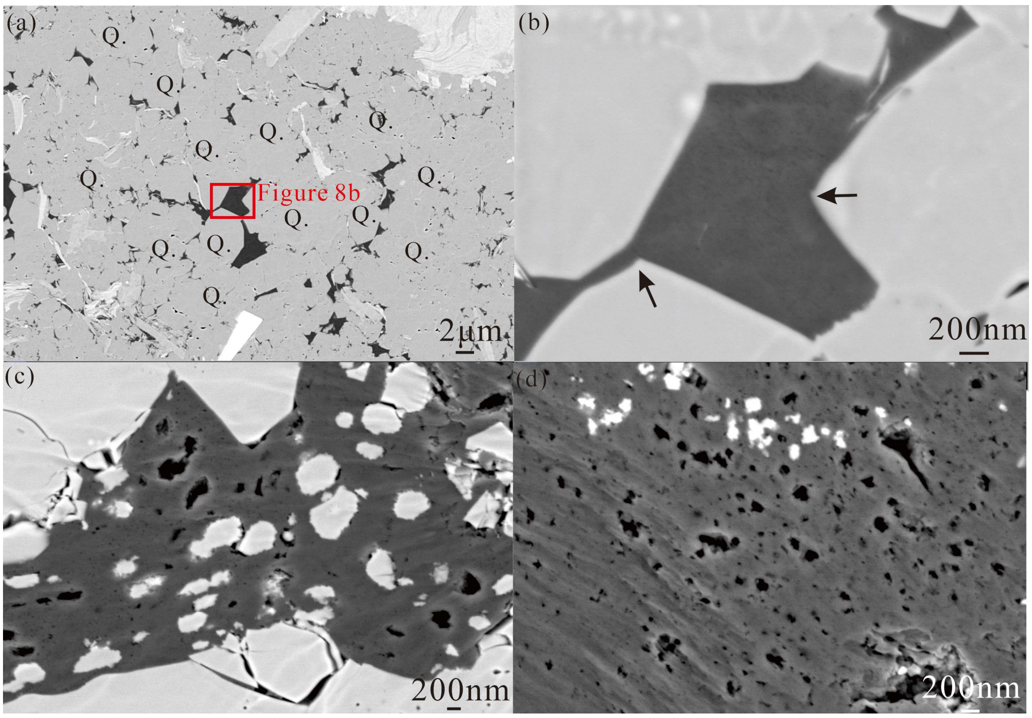

Figure 8. OM pores hosted by pyrobitumen: (**a**,**b**) pyrobitumen filling the interparticle pores among authigenic quartz hosting abundant pores. Black arrows in Figure 8b point to the euhedral termination of authigenic quartz. (**c**,**d**) Abundant pores hosted by massive pyrobitumen. Some pores are filled with authigenic minerals, including pyrite and apatite.

Pyrobitumen filling the interparticle pores within pyrite framboids hosts abundant pores of three types (Figure 6c). The first type is similar to pores hosted by pyrobitumen filling the interstitial spaces between authigenic quartz grains. The morphology and size of pores of the second type are those of single crystals of framboidal pyrite. It is possible that some of these pores were produced by the plucking of pyrite crystals during sample preparation. These pores, some of which may be artificial, have been referred to as "moldic pores" by some researchers [43]. The third type of OM pores is crescent-shaped voids at some contacts of pyrite crystals.

Pyrobitumen filling the interparticle pores at contacts of clay grains contains abundant pores of differing morphology, size, and distribution (Figure 6d). Some pores exhibit an obvious directional arrangement, some are circular or elliptical, some are flat, some pores appear to be restricted to the middle of the OM, and some are concentrated along the contacts between OM and clay minerals.

Massive pyrobitumen contains abundant pores that can be categorized into three types (Figures 7 and 8c,d). The first type of pores hosted by massive pyrobitumen is similar to pores contained by pyrobitumen filling the interstitial spaces between authigenic quartz grains. These pores are equal sized and circular or elliptical (Figures 7b and 8d). The second type of pores is large and irregular in shape and partially filled with authigenic minerals, mainly pyrite and apatite. The third type of pores is formed at the contacts of minerals and OM particles (Figure 7a,d).

4.3. Implications for Diagenetic History

Deposits of the Wufeng and Longmaxi Formations contain abundant authigenic quartz (Figures 6a, 8b and 9), especially the former [36]. Previous studies have pointed out that the silica of this kind of quartz, largely derived by the dissolution of siliceous organisms, such as radiolaria, forms early in the diagenetic burial history of the sediment [44,45]. Pyrobitumen, however, is generally produced in the middle and late diagenetic stages. Early formed authigenic quartz occupies most of the primary porosity as cement. However, its high rigidity shields and preserves some depositional porosity, thus providing space for the subsequent migration of pyrobitumen. Similarly, framboidal pyrite generally forms in the early diagenetic stage, earlier than the time of formation of pyrobitumen. Therefore, the morphology of pyrobitumen reflects the shapes of the pores it has filled.

The pore-filling sequence for authigenic clay minerals and pyrobitumen remains elusive. We observed that authigenic clay minerals filled pores in some samples with a high TOC content that lack pyrobitumen (Figure 9a,b). Thus, we infer that authigenic clay minerals preferentially filled pores and created pores of a small throat size so that the driving force of pyrobitumen migration was not enough to overcome the resistance caused by the small pore throat dimensions. Little pyrobitumen has filled small interparticle pores formed at contacts of authigenic quartz (Figure 9c). In contrast, some large interparticle pores preserved by authigenic quartz are often filled with pyrobitumen (Figures 6a and 8a). These observations provide some support for the inference that pyrobitumen was unable to migrate through small pores and throats. It is worth pointing out that some researchers have suggested that authigenic clay minerals may form earlier than the migration of OM and that the dimensions of pore throats are altered by the formation of authigenic clay minerals [46,47].

Pores formed in OM in association with thermal maturation are important to the storage volume of a shale gas reservoir [48,49]. However, the characteristics of OM-hosted pores in the various types of pyrobitumen display notable differences. Small, equal-sized pores of circular or oval shape are the most common type of OM pores in the studied samples (Figures 6b, 7b and 8b). Clay minerals comprise an especially plastic component of shale deposits. The mechanical compaction of clay-rich deposits causes existing pores to close. Fishman et al. (2012) pointed out that although the Upper Jurassic Kimmeridge Clay Formation shale has a high OM content, the large amount of clay minerals present has negated the reservoir potential of these rocks [50]. Pores hosted in OM that formed as a result of thermal maturation are poorly preserved and difficult to discern even using SEM. However, there is a greater chance for the preservation of OM pores in deposits containing abundant authigenic quartz and pyrite because of the strong rigidity of these minerals.

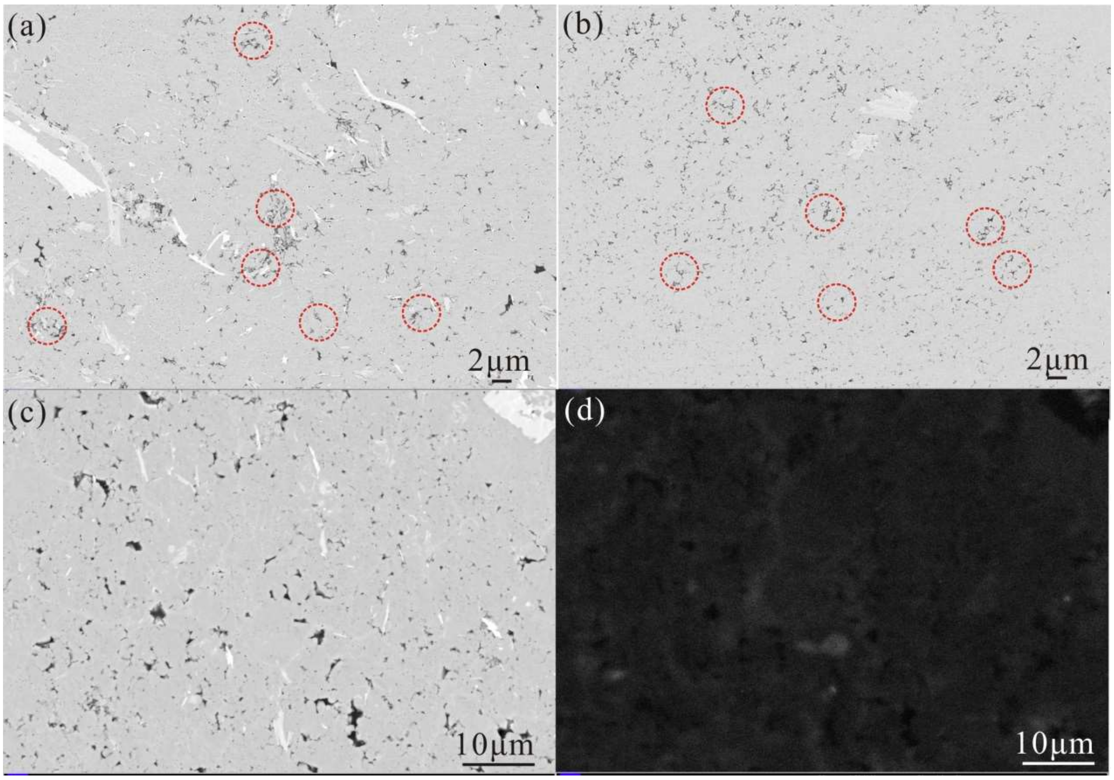

Figure 9. Authigenic quartz of Wufeng–Longmaxi Formation samples: (**a**) authigenic quartz widely distributed throughout the clay matrix. Red circles indicate where clay minerals have filled the interparticle pores among authigenic quartz. (**b**) Authigenic quartz is widely distributed throughout the clay matrix. Red circles indicate interparticle pores of authigenic quartz that lack OM and other minerals. (**c**) Authigenic quartz widely distributed throughout the clay matrix. Interparticle pores among authigenic quartz lack OM and mineral fillings. (**d**) Cathodoluminescence image of the same field of view as (**c**). Note that the authigenic quartz displays no more than weak cathodoluminescence.

Massive pyrobitumen hosts pores that are similar to those contained by pyrobitumen filling the interstitial spaces among authigenic quartz grains (Figure 7b). Still, meager large, unevenly shaped pores have also been observed in massive pyrobitumen (Figures 7d,f and 8c). Some of the large and unevenly shaped OM pores are filled with authigenic minerals, with the morphology of the pore-filling minerals reflecting the morphology of the pores. Therefore, these OM pores appear to have formed prior to the authigenic minerals. However, further study is required to make certain that these OM pores are actually unfilled or moldic pores formed during sample preparation. Our investigation indicates that such pores in massive pyrobitumen are obviously different from moldic pores. The latter are closed at one end (Figure 6c), whereas the pores hosted by the massive pyrobitumen of the studied samples appear to be connected (Figures 7f and 8c).

Differences in OM pores can be observed in adjacent grains of massive pyrobitumen (Figure 7a). One grain displays abundant equal-sized pores that are not filled with minerals. The other grain contains pores that are filled with minerals. This observation may indicate that the two types of OM pores formed at different times. The large OM pores may have formed earlier than authigenic minerals, and authigenic minerals may have precipitated earlier than smaller OM pores forming. Small OM pores are thought to form in large numbers in association with the gas generation stage, whereas the time of formation of large OM pores can be roughly judged by the timing of filling with authigenic minerals (mostly pyrite).

We can provide a tentative speculative explanation for the features described earlier. The relatively large pores hosted by OM may be depositional. A number of studies have made the case that immature OM, including amorphous OM and OM displaying special structures (e.g., algae and animal debris), will host many pores [11,51]. Our observations of the Wufeng and Longmaxi samples indicate that large OM pores filled with authigenic minerals are present only in the massive pyrobitumen; they are not present in pyrobitumen types displaying evidence of migration. The primary pores may have been severely deformed or closed after significant mechanical compaction (depth of burial). Indeed, the abundance of OM pores may have diminished with increasing burial depth because of the ductile nature of OM. OM pores may survive burial as a result of their infilling with authigenic minerals or solid bitumen, which is associated with high levels of thermal maturity [51]. This mechanism may explain why some OM pores have been filled with minerals and others have not been filled. It may offer an explanation for the strong heterogeneity of OM pore development in adjacent OM particles.

Generally speaking, the type of OM is an endogenous factor that may be a determinant in the development of OM pores, whereas diagenesis is an exogenous factor affecting the preservation of OM pores. The combinations of these endogenous and exogenous factors govern the distribution of OM and the heterogeneity of OM pore development in shale.

4.4. Implications for Shale Gas Exploration

Although organic-rich shale deposits have been documented from marine, lacustrine, and marine–continental transitional facies (coal measures), marine shale deposits have been most successfully exploited for commercial purposes in China. The abundance of OM is the basis of shale gas enrichment and is an important basis for optimizing shale successions. In addition to the abundance of OM, the OM type and the nature of the association of OM with minerals should be taken into account when assessing reservoir rock quality.

The Ordovician–Silurian Wufeng–Longmaxi Formations and the Lower Cambrian Niutitang Formation of the Sichuan Basin and surrounding areas, southern China, offer great potential for hydrocarbon exploration and production. These formations host prospective types of OM and promising mineralogy and grain arrangements [25,30,52]. Pyrobitumen is the dominant type of OM and mainly occurs as fillings of interparticle pores among authigenic quartz (Figure 10). The early formed authigenic quartz has shielded the pores from the effects of mechanical compaction, ensuring that a large number of pores hosted by OM are preserved. This has provided sufficient reservoir storage space for shale gas. In addition, the abundant authigenic quartz has made the shale brittle and more susceptible to fracturing [35,53].

Coal measure shale deposits commonly have a high thermal maturity and abundance of OM. Good examples of coal measures in China include the Carboniferous–Permian Taiyuan–Shanxi Formations of the Ordos and Qinshui Basins and the Permian Longtan Formation of the Sichuan Basin [54–56]. However, coal measure shale is characterized by a high clay mineral content and lack rigid minerals, both of which diminish the preservation potential of OM pores (Figure 10). Moreover, the fact that much of the OM in coal measure shales comes from higher plants (vitrinite and inertinite) diminishes the hydrocarbon generation potential of these deposits (Gai et al., 2018) as well as the potential of the development of OM pores [57]. Thus, the development prospects for these shales are much lower than those of marine shale.

Organic-rich lacustrine shale deposits include the Triassic Yanchang Formation of the Ordos Basin and the Upper Cretaceous Qingshankou Formation of the Songliao Basin [58,59]. The dominant OM of lacustrine shale is derived from lower organisms. The thermal maturity of these deposits in China is typically low, generally no greater than the oil window stage. The OM contained in these deposits is mainly solid bitumen that occupies residual porosity (Figure 10). OM pores are not especially well developed in solid bitumen because of low thermal maturity.

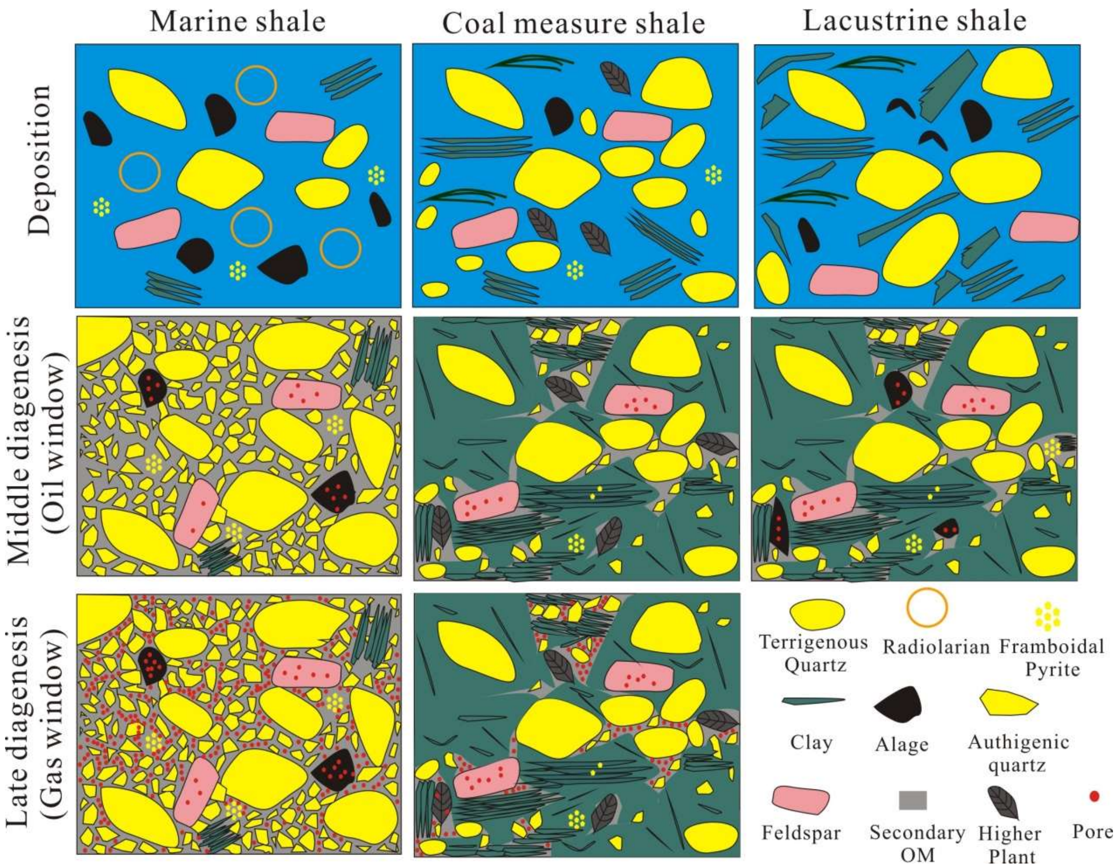

Figure 10. Sketch of grain assemblages (mainly quartz and OM types) and diagenesis of marine shale, coal measure shale, and lacustrine shale (modified after [35]). Note that marine shale refers to shale with geological characteristics similar to those of the Wufeng–Longmaxi Formations, deposited on the upper Yangtze Platform. Coal measure shale refers to shale with geological characteristics similar to those of the Carboniferous–Permian Taiyuan and Shanxi Formations that were deposited in the Qinshui or Ordos Basins. Lacustrine shale refers to shale with geological characteristics similar to those of the Triassic Yanchang Formation that accumulated in the Ordos Basin. Refer to the text for further discussion.

The type of OM in marine shale and its mode of grain-to-grain relationships with minerals are mainly controlled by the sedimentary environment. For example, the most favorable interval of the Wufeng–Longmaxi succession in the study area encompasses Katian and Rhuddanian shales [60,61]. These deposits appear to have accumulated in deep water under reducing conditions beneath highly productive surface water [61]. These characteristics are conducive to the enrichment of sediment with OM and siliceous tests, the requisites for the formation of organic-rich siliceous shale (Figure 11a,b). Aeronian shale accumulated under more oxygenated and shallow conditions beneath surface water that was not productive (Figure 11c). The change in the sedimentary environment is manifested by the transformation from Katian and Rhuddanian organic- and silica-rich shale to Aeronian shales enriched in clay and depleted of OM (Figure 11). The changing depositional conditions gave rise to different types of OM and modes of occurrence of OM with mineral assemblages. This in turn affected the quality of the present shale gas reservoir. A suitable sedimentary environment is therefore a prerequisite for the formation of high-quality shale for hydrocarbon generation (viz., the abundance of OM, type of OM, and its combination with minerals).

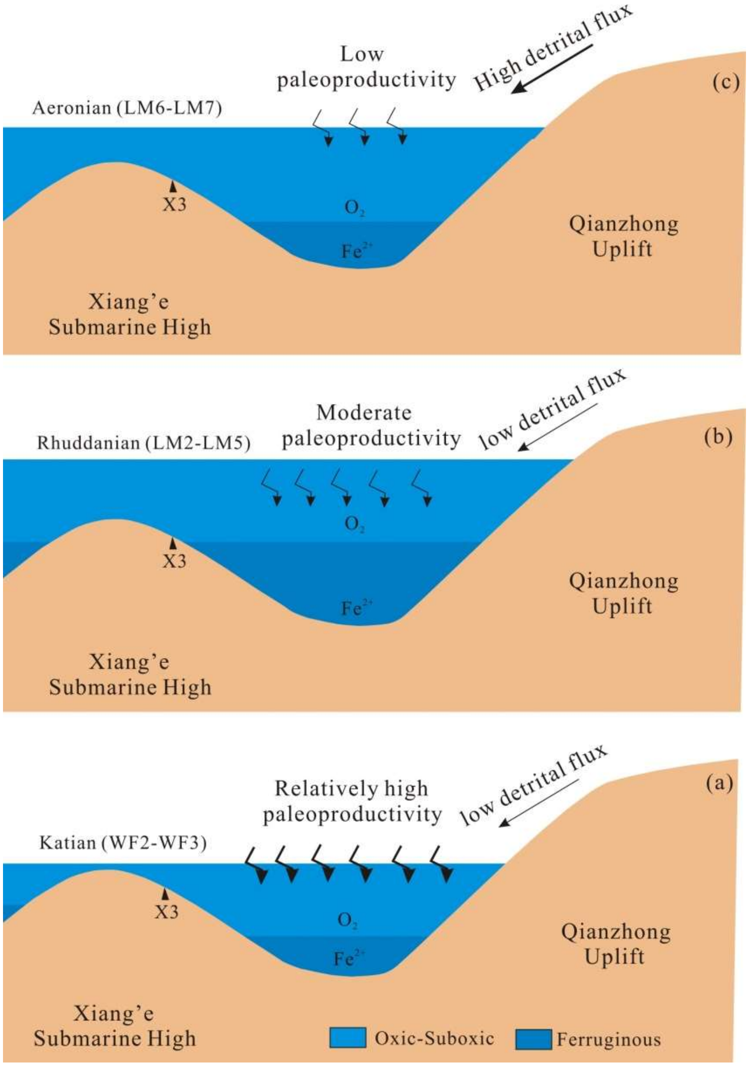

Figure 11. Sedimentary model of the Katian–Aeronian stages of basin evolution (modified after [34]): (**a**) Katian stage, (**b**) Rhuddanian stage, and (**c**) Aeronian stage. The data of redox conditions, paleoproductivity, and detrital flux for well X3 located in the study area are from [34].

5. Conclusions

The type of OM contained in marine shale of the studied Wufeng and Longmaxi Formations is mainly pyrobitumen, with lesser amounts of graptolite and OM of unknown origin. SEM analysis indicates that the pyrobitumen of the investigated samples exists in four forms: massive material, the filling of interparticle pores at contacts of quartz grains, the filling of interparticle pores within pyrite framboids, and the filling of interparticle pores at contacts of authigenic clay mineral.

The development of OM pores in deposits of the Wufeng–Longmaxi succession was affected by the type of OM and degree of diagenesis. The morphology, size, and time of formation of OM pores appear to be a function of OM type. The most common OM pores hosted by pyrobitumen are small, equal-sized, circular or oval pores. These pores represent the main storage volume of the studied deposits.

The type of OM and its mode of co-occurrence with minerals affect the quality of the shale gas reservoir. Pyrobitumen of the studied Wufeng and Longmaxi samples, especially the former, filled the interparticle pores among authigenic quartz. These deposits are characterized by robust reservoir capacity and fracturing capacity. The type of OM and mode of its grain-to-grain association with minerals are mainly controlled by the sedimentary environment. An appropriate sedimentary environment is therefore a prerequisite for the formation of high-quality shale for hydrocarbon generation and storage.

Shale is rich in organic matter, but its types are diverse. It is necessary to strengthen the research on basic geological data and find OM type evaluation methods that are more suitable for geological characteristics in order to lead the healthy and sustainable development of the shale gas industry.

Author Contributions: Conceptualization, J.W. and Z.X.; methodology, J.W. and Z.X.; validation and formal analysis, F.Y.; writing—original draft preparation, J.W. and Z.X.; writing—review and editing, J.W., G.G.L. and Z.X.; funding acquisition, Z.X. All authors have read and agreed to the published version of the manuscript.

Funding: This research received no external funding.

Data Availability Statement: Data are unavailable due to privacy or ethical restrictions.

Acknowledgments: We greatly thank the editors and reviewers for their critical comments and valuable suggestions, which were helpful to improve the manuscript. This work was supported by the National Natural Science Foundation of China (No. 42302203).

Conflicts of Interest: The authors declare no conflict of interest.

References

1. Curtis, J.B. Fractured shale-gas systems. *AAPG Bull.* **2002**, *86*, 1921–1938.
2. Bustin, R.M.; Bustin, A.; Ross, D. Shale gas opportunities and challenges. *Search Discov. Artic.* **2015**, *40382*, 20–23.
3. Zou, C.N.; Dong, D.Z.; Wang, Y.M.; Li, X.J.; Huang, J.L.; Wang, S.F.; Guan, Q.Z.; Zhang, C.C.; Wang, H.Y.; Liu, H.L.; et al. Shale gas in China: Characteristics, challenges and prospects (II). *Pet. Explor. Dev.* **2018**, *43*, 182–196. [CrossRef]
4. Pang, X.Q.; Jia, C.Z.; Chen, J.Q.; Li, M.W.; Wang, W.Y.; Hu, Q.H.; Guo, Y.C.; Chen, Z.X.; Peng, J.W.; Liu, K.Y.; et al. A unified model for the formation and distribution of both conventional and unconventional hydrocarbon reservoirs. *Geosci. Front.* **2021**, *12*, 695–711. [CrossRef]
5. Hao, F.; Zou, H.Y.; Lu, Y.C. Mechanisms of shale gas storage: Implications for shale gas exploration in China. *AAPG Bull.* **2013**, *97*, 1325–1346. [CrossRef]
6. Dang, W.; Zhang, J.; Tang, X.; Chen, Q.; Han, S.; Li, Z.; Du, X.; Wei, X.; Zhang, M.; Liu, J.; et al. Shale gas potential of Lower Permian marine-continental transitional black shales in the Southern North China Basin, central China: Characterization of organic geochemistry. *J. Nat. Gas. Sci. Eng.* **2016**, *28*, 639–650. [CrossRef]
7. Xi, Z.D.; Tang, S.H.; Wang, J.; Yang, G.Q.; Li, L. Formation development of pore structure in marine-continental transitional shale from northern China across a maturation gradient: Insights from gas adsorption mercury intrusion. *Int. J. Coal Geol.* **2018**, *200*, 87–102. [CrossRef]
8. Tissot, B.P.; Welte, D.H. *Petroleum Formation and Occurrence: A New Approach to Oil and Gas Exploration*; Springer-Verlag: Berlin, Germany, 1978.
9. Loucks, R.G.; Reed, R.M.; Ruppel, S.C.; Jarvie, D.M. Morphology genesis distribution of nanometer-scale pores in siliceous mudstones of the Mississippian Barnett shale. *J. Sediment. Res.* **2009**, *79*, 848–861. [CrossRef]
10. Loucks, R.G.; Reed, R.M.; Ruppel, S.C.; Hammes, U. Spectrum of pore types and networks in mudrocks and a descriptive classification for matrix-related mudrock pores. *AAPG Bull.* **2012**, *96*, 1071–1098. [CrossRef]
11. Milliken, K.L.; Ko, L.T.; Pommer, M.; Marsaglia, K.M. SEM Petrography of Eastern Mediterranean Sapropels: Analogue Data for Assessing Organic Matter In Oil and Gas Shales. *J. Sediment. Res.* **2014**, *84*, 961–974. [CrossRef]
12. Valentine, B.J.; Hackley, P.C. Applications of correlative light and electron microscopy (CLEM) to organic matter in the North American shale petroleum systems. *AAPG Mem.* **2019**, *120*, 1–18.
13. Xi, Z.; Tang, S.; Li, J.; Zhang, Z.; Xiao, H. Pore characterization and the controls of organic matter and quartz on pore structure: Case study of the Niutitang Formation of northern Guizhou Province, South China. *J. Nat. Gas. Sci. Eng.* **2019**, *61*, 18–31. [CrossRef]
14. Mastalerz, M.; Drobniak, A.; Stankiewicz, A.B. Origin properties implications of solid bitumen in source-rock reservoirs: A review. *Int. J. Coal Geol.* **2018**, *195*, 14–36. [CrossRef]
15. Zhang, H.; Jiao, S.J.; Pang, Q.F.; Li, N.; Lin, B.W. SEM observation of organic matters in the Eopaleozoic shale in South China. *Oil Gas Geol.* **2015**, *36*, 675–680.
16. Loucks, R.G.; Reed, R.M. Scanning-electron-microscope petrographic evidence for distinguishing organic-matter pores associated with depositional organic matter versus migrated organic matter in mudrock. *Gulf Coast Assoc. Geol. Soc. J.* **2014**, *3*, 51–60.
17. Zhao, J.H.; Jin, Z.J.; Jin, Z.K.; Hu, Q.H.; Hu, Z.Q.; Du, W.; Yan, C.N.; Geng, Y.K. Mineral types and organic matters of the Ordovician-Silurian Wufeng and Longmaxi Shale in the Sichuan Basin, China: Implications for pore systems, diagenetic pathways, and reservoir quality in fine-grained sedimentary rocks. *Mar. Petrol. Geol.* **2017**, *86*, 655–674. [CrossRef]

18. Camp, W.K. Diagenetic evolution of organic matter cements: Implications for unconventional shale reservoir quality prediction. *AAPG Mem.* **2019**, *120*, 209–224.
19. Hackley, P.C.; Cardott, B.J. Application of organic petrography in North American shale petroleum systems: A review. *Int. J. Coal Geol.* **2016**, *163*, 8–51. [CrossRef]
20. Curiale, J.A. Origin of solid bitumens, with emphasis on biological marker results. *Org. Geochem.* **1986**, *10*, 559–580. [CrossRef]
21. Curiale, J.A.; Curtis, J.B. Organic geochemical applications to the exploration for source-rock reservoirs: A review. *J. Unconv. Oil Gas Res.* **2016**, *13*, 1–31. [CrossRef]
22. Hackley, P.C.; Valentine, B.J.; Voortman, L.M.; Van Oosten Slingeland, D.S.B.; Hatcherian, J. Utilization of integrated correlative light electron microscopy (iCLEM) for imaging sedimentary organic matter. *J. Microsc.* **2017**, *267*, 371–383. [CrossRef] [PubMed]
23. Liu, B.; Mastalerz, M.; Schieber, J. SEM petrography of dispersed organic matter in black shales: A review. *Earth-Sci. Rev.* **2022**, *224*, 103874. [CrossRef]
24. Teng, J.; Liu, B.; Mastalerz, M.; Schieber, J. Origin of organic matter and organic pores in the overmature Ordovician-Silurian Wufeng-Longmaxi Shale of the Sichuan Basin, China. *Int. J. Coal Geol.* **2022**, *253*, 103970. [CrossRef]
25. Zhao, W.; Li, J.; Yang, T.; Wang, S.; Huang, J. Geological difference and its significance of marine shale gases in South China. *Petrol. Explor. Develop.* **2016**, *43*, 547–559. [CrossRef]
26. Tan, J.; Horsfield, B.; Fink, R.; Krooss, B.; Schulz, H.M.; Rybacki, E.; Zhang, J.; Boreham, J.C.; van Graas, G.; Tocher, B.A. Shale Gas Potential of the Major Marine Shale Formations in the Upper Yangtze Platform, South China, Part III: Mineralogical, Lithofacial, Petrophysical, and Rock Mechanical Properties. *Energy Fuels* **2014**, *28*, 2322–2342. [CrossRef]
27. Ma, Y.S.; Cai, X.Y.; Zhao, P. China's shale gas exploration and development: Understanding and practice. *Petrol. Explor. Develop.* **2018**, *45*, 589–603. [CrossRef]
28. Nie, H.K.; He, Z.L.; Liu, G.X.; Zhang, G.R.; Lu, Z.Y.; Li, D.H.; Sun, C.X. Status and direction of shale gas exploration and development in China. *J. China Univ. Min. Technol.* **2020**, *49*, 13–35.
29. Qiu, Z.; Zou, C.N. Unconventional petroleum sedimentology: Connotation and prospect. *Acta Sedimentol. Sin.* **2020**, *38*, 1–29.
30. Zou, C.N.; Yang, Z.; Sun, S.S.; Zhao, Q.; Bai, W.H.; Liu, H.L.; Pan, S.Q.; Wu, S.T.; Yuan, Y.L. "Exploring petroleum inside source kitchen": Shale oil and gas in Sichuan Basin. *Sci. China Earth Sci.* **2020**, *63*, 934–953. [CrossRef]
31. Li, Y.F.; Schieber, J.; Fan, T.L.; Wei, X.J. Pore characterization and shale facies analysis of the Ordovician-Silurian transition of northern Guizhou, South China: The controls of shale facies on pore distribution. *Mar. Petrol. Geol.* **2018**, *92*, 697–718. [CrossRef]
32. Yang, C.; Xiong, Y.Q.; Zhang, J.C. A comprehensive re-understanding of the OM-hosted nanopores in the marine Wufeng–Longmaxi shale formation in South China by organic petrology gas adsorption X-ray diffraction studies. *Int. J. Coal Geol.* **2020**, *218*, 103362. [CrossRef]
33. Qiu, Z.; Liu, B.; Dong, D.; Lu, B.; Yawar, Z.; Chen, Z.; Schieber, J. Silica diagenesis in the Lower Paleozoic Wufeng and Longmaxi Formations in the Sichuan Basin, South China: Implications for reservoir properties and paleoproductivity. *Mar. Pet. Geol.* **2020**, *121*, 104594. [CrossRef]
34. Xi, Z.D.; Tang, S.H.; Lash, G.G.; Zhang, B.; Lin, D.L. Geochemical characteristics of organic carbon and pyrite sulfur in Ordovician-Silurian transition shales in the Yangtze Platform, South China: Implications for the depositional environment. *Palaeogeogr. Palaeoclimatol. Palaeoecol.* **2021**, *563*, 110173. [CrossRef]
35. Xi, Z.D.; Tang, S.H.; Lash, G.G.; Ye, Y.P.; Lin, D.L.; Zhang, B. Depositional controlling factors on pore distribution and structure in the lower Silurian Longmaxi shales: Insight from geochemistry and petrology. *Mar. Petrol. Geol.* **2021**, *130*, 105114. [CrossRef]
36. Wang, Q.T.; Wang, T.L.; Liu, W.P.; Zhang, J.; Feng, Q.; Lu, H.; Peng, P.A. Relationships among composition, porosity and permeability of Longmaxi shale reservoir in the weiyuan block, Sichuan Basin, China. *Mar. Petrol. Geol.* **2019**, *102*, 33–47. [CrossRef]
37. Lu, Y.B.; Jiang, S.; Lu, Y.C.; Xu, S.; Wang, Y.X. Productivity or preservation? The factors controlling the organic matter accumulation in the late Katian through Hirnantian Wufeng organic-rich shale, South China. *Mar. Petrol. Geol.* **2019**, *109*, 22–35. [CrossRef]
38. Zhang, L.C.; Li, B.; Jiang, S.; Xiao, D.S.; Lu, S.F.; Zhang, Y.Y.; Gong, C.; Chen, L. Heterogeneity characterization of the lower Silurian Longmaxi marine shale in the Pengshui area, South China. *Int. J. Coal Geol.* **2018**, *195*, 250–266. [CrossRef]
39. Guo, X.W.; Qin, Z.J.; Yang, R.; Dong, T.; He, S.; Hao, F.; Yi, J.Z.; Shu, Z.G.; Bao, H.Y.; Liu, K.Y. Comparison of pore systems of clay-rich and silica-rich gas shales in the lower Silurian Longmaxi formation from the Jiaoshiba area in the eastern Sichuan Basin, China. *Mar. Pet. Geol.* **2019**, *101*, 265–280. [CrossRef]
40. Misch, D.; Gross, D.; Hawranek, G.; Horsfield, B.; Klaver, J.; Mendez-Martin, F.; Urai, J.L.; Vranjes-Wessely, S.; Sachsenhofer, R.F.; Schmatz, J.; et al. Solid bitumen in shales: Petrographic characteristics implications for reservoir characterization. *Int. J. Coal Geol.* **2019**, *205*, 14–31. [CrossRef]
41. Wood, J.M.; Sanei, H.; Haeri-Ardakanic, O.; Curtis, M.E.; Akaie, T.; Currie, C. Solid bitumen in the Montney Formation: Diagnostic petrographic characteristics significance for hydrocarbon migration. *Int. J. Coal Geol.* **2018**, *198*, 48–62. [CrossRef]
42. Reyes, J.; Jiang, C.; Lavoie, D.; Armstrong, D.K.; Milovic, M.; Robinson, R. Organic petrographic analysis of artifcially matured chitinozoan-and graptolite-rich upper Ordovician shale from Hudson Bay Basin, Canada. *Int. J. Coal Geol.* **2018**, *199*, 138–151. [CrossRef]
43. Pommer, M.; Milliken, K. Pore types and pore-size distributions across thermal maturity, Eagle Ford Formation, southern Texas. *Am. Assoc. Pet. Geol. Bull.* **2015**, *99*, 1713–1744. [CrossRef]

44. Peng, J.W.; Milliken, K.L.; Fu, Q.L. Quartz types in the Upper Pennsylvanian organic-rich Cline Shale (Wolfcamp D), Midland Basin, Texas: Implications for silica diagenesis, porosity evolution and rock mechanical properties. *Sedimentology* **2020**, *67*, 2040–2064. [CrossRef]
45. Gao, P.; Xiao, X.; Hu, D.; Lash, G.G.; Liu, R.; Cai, Y.; Wang, Z.; Zhang, B.; Yuan, T.; Liu, S. Effect of silica diagenesis on porosity evolution of deep gas shale reservoir of the Lower Paleozoic Wufeng-Longmaxi formations, Sichuan Basin. *Mar. Pet. Geol.* **2022**, *145*, 105873. [CrossRef]
46. Schneider, J.; Flemings, P.; Day-Stirrat, R.; Germaine, J.T. Insights into pore-scale controls on mudstone permeability through resedimentation experiments. *Geology* **2011**, *39*, 1011–1014. [CrossRef]
47. Zhu, H.J.; Ju, Y.W.; Yang, M.P.; Huang, C.; Feng, H.; Qiao, P.; Ma, C.; Su, X.; Lu, Y.J.; Shi, E.X.; et al. Grain-scale petrographic evidence for distinguishing detrital and authigenic quartz in shale: How much of a role do they play for reservoir property and mechanical characteristic? *Energy* **2022**, *239*, 122176. [CrossRef]
48. Wang, R.Y.; Hu, Z.Q.; Long, S.X. Differential characteristics of the Upper Ordovician-Lower Silurian Wufeng-Longmaxi shale reservoir and its implications for exploration and development of shale gas in/around the Sichuan Basin. *Acta Geol. Sin. (Engl. Ed.)* **2019**, *93*, 520–535. [CrossRef]
49. Wang, R.Y.; Hu, Z.Q.; Long, S.X. Reservoir characteristics and evolution mechanisms of the Upper Ordovician Wufeng-Lower Silurian Longmaxi shale, Sichuan Basin. *Oil Gas Geol.* **2022**, *43*, 353–364.
50. Fishman, N.S.; Hackley, P.C.; Lowers, H.A.; Hill, R.J.; Egenhoff, S.O.; Eberl, D.D.; Blum, A.E. The nature of porosity in organic-rich mudstones of the Upper Jurassic Kimmeridge Clay Formation, North Sea, offshore United Kingdom. *Int. J. Coal Geol.* **2012**, *103*, 32–50. [CrossRef]
51. Löhr, S.C.; Baruch, E.T.; Hall, P.A.; Kennedy, M.J. Is organic pore development in gas shales influenced by the primary porosity and structure of thermally immature organic matter? *Org. Geochem.* **2015**, *87*, 119–132. [CrossRef]
52. Wang, Y.X.; Xu, S.; Hao, F.; Zhang, B.Q.; Shu, Z.G.; Gou, Q.Y.; Lu, Y.B.; Cong, F.Y. Multiscale petrographic heterogeneity and their implications for the nanoporous system of the Wufeng-Longmaxi shales in Jiaoshiba area, Southeast China: Response to depositional-diagenetic process. *GSA Bull.* **2020**, *132*, 1704–1721. [CrossRef]
53. Jarvie, D.M.; Hill, R.J.; Ruble, T.E.; Pollastro, R.M. Unconventional shale-gas systems: The Mississippian Barnett Shale of North-central Texas as one model for thermogenic shale-gas assessment. *AAPG Bull.* **2007**, *91*, 475–499. [CrossRef]
54. Wei, J.Y.; Wang, Y.L.; Wang, G.; Wei, Z.F.; He, W. Geochemistry and shale gas potential of the lower Permian marine-continental transitional shales in the Eastern Ordos Basin. *Energy Explor. Exploit.* **2021**, *39*, 738–760. [CrossRef]
55. Liu, H.H.; Yumina, D.D.; Liu, J.L.; Hu, B.L.; Xu, H.J.; Wu, H.Y.; Shang, J.H.; Zheng, K.G.; Wei, Q.; Zhang, M.; et al. Preliminary Assessment of the Resource and Exploitation Potential of Lower Permian Marine-Continent Transitional Facies Shale Gas in the Huainan Basin, Eastern China, Based on a Comprehensive Understanding of Geological Conditions. *ACS Omega* **2021**, *6*, 8502–8516. [CrossRef] [PubMed]
56. Yang, H.Z.; Lin, L.B.; Chen, L.Q.; Yu, Y.; Li, D.; Tian, J.C.; Zhou, W.; He, J.H. Characteristics of Mineralogy, Lithofacies of Fine-Grained Sediments and Their Relationship with Sedimentary Environment: Example from the Upper Permian Longtan Formation in the Sichuan Basin. *Energies* **2021**, *14*, 3662. [CrossRef]
57. Gai, H.F.; Tian, H.; Xiao, X.M. Late gas generation potential for different types of shale source rocks: Implications from pyrolysis experiments. *Int. J. Coal Geol.* **2018**, *193*, 16–29. [CrossRef]
58. Luo, Q.Y.; Zhong, N.N.; Dai, N.; Zhang, W. Graptolite-derived organic matter in the Wufeng–Longmaxi Formations (Upper Ordovician–Lower Silurian) of southeastern Chongqing, China: Implications for gas shale evaluation. *Int. J. Coal Geol.* **2016**, *153*, 87–98. [CrossRef]
59. Xiao, L.; Li, Z.; Hou, Y.F.; Xu, L.; Wang, L.W.; Yang, Y.D. Characteristics of Organic Macerals and Their Influence on Hydrocarbon Generation and Storage: A Case Study of Continental Shale of the Yanchang Formation from the Ordos Basin, China. *Geofluids* **2021**, *2021*, 5537154. [CrossRef]
60. Huang, H.Y.; He, D.F.; Li, D.; Li, Y.Q.; Zhang, W.K.; Chen, J.J. Geochemical characteristics of organic-rich shale, Upper Yangtze Basin: Implications for the Late Ordovician-Early Silurian orogeny in South China. *Palaeogeogr. Palaeoclimatol. Palaeoecol.* **2020**, *554*, 109822. [CrossRef]
61. Li, N.; Li, C.; Fan, J.X.; Algeo, T.J.; Yan, D.T.; Zhu, G.Y.; Wu, S.Y.; Tang, S.D.; Cheng, M.; Jin, C.S. Sulfate-controlled marine euxinia in the semi-restricted inner Yangtze Sea (South China) during the Ordovician-Silurian transition. *Palaeogeogr. Palaeoclimatol. Palaeoecol.* **2019**, *534*, 109281. [CrossRef]